

Measurements of Cosmic-ray Low-energy Antiproton and Proton Spectra in a Transient Period of the Solar Field Reversal

Y. Asaoka¹, Y. Shikaze¹, K. Abe¹, K. Anraku¹, M. Fujikawa¹, H. Fuke¹, S. Haino¹, M. Imori¹, K. Izumi¹, T. Maeno², Y. Makida³, S. Matsuda¹, N. Matsui¹, T. Matsukawa², H. Matsumoto¹, H. Matsunaga^{1,†}, J. Mitchell⁴, T. Mitsui^{2,‡}, A. Moiseev⁴, M. Motoki^{1,‡}, J. Nishimura¹, M. Nozaki², S. Orito^{1,*}, J. F. Ormes⁴, T. Saeki¹, T. Sanuki¹, M. Sasaki³, E. S. Seo⁵, T. Sonoda¹, R. Streitmatter⁴, J. Suzuki³, K. Tanaka³, K. Tanizaki², I. Ueda¹, J. Z. Wang⁵, Y. Yajima⁶, Y. Yamagami⁶, A. Yamamoto³, Y. Yamamoto¹, K. Yamato², T. Yoshida³, and K. Yoshimura³

¹*The University of Tokyo, Tokyo, 113-0033 JAPAN*

²*Kobe University, Kobe, Hyogo, 657-8501 JAPAN*

³*High Energy Accelerator Research Organization (KEK), Tsukuba, Ibaraki 305-0801, JAPAN*

⁴*National Aeronautics and Space Administration, Goddard Space Flight Center (NASA/GSFC), Greenbelt, MD 20771, USA*

⁵*University of Maryland, College Park, MD 20742, USA*

⁶*The Institute of Space and Astronautical Science (ISAS), Sagami-hara, Kanagawa 229-8510, JAPAN*

(October 24, 2018)

The energy spectra of cosmic-ray low-energy antiprotons (\bar{p} 's) and protons (p 's) have been measured by BESS in 1999 and 2000, during a period covering the solar magnetic field reversal. Based on these measurements, a sudden increase of the \bar{p}/p flux ratio following the solar magnetic field reversal was observed, and it generally agrees with a drift model of the solar modulation.

PACS numbers: 98.70.Sa, 96.40.Kk, 95.85.Ry

Much of the real underlying physics of the Sun is related to the 22 yr solar magnetic cycle with recurrent positive and negative phases. The magnetic field polarity reverses when the solar activity is maximum, and the global magnetic field profile reverses in the heliosphere. The most recent field reversal happened in the beginning of 2000. The solar modulation of cosmic rays is caused by expanding solar wind, which spreads out locally irregular magnetic field and therefore modifies energy spectra of the cosmic rays entering the heliosphere. The positive and negative particles drift in opposite directions, taking different routes to arrive at the Earth in the heliospheric magnetic field. The charge-sign dependence is, therefore, a natural consequence [1], on top of the common time dependent change in the overall modulation. It explains alternate appearances of "flat" and "peaked" periods in neutron monitor data around solar minima. Recent works [2–4] also indicated that the drift produces non-negligible effects between the positive and negative particles even during the high solar activity. This view is supported by measurements of temporal variation in cosmic-ray ratios [5], such as electrons to helium nuclei (He) and electrons to protons (p 's), where the largest variation is associated with the solar magnetic field reversal. Among various cosmic-ray pairs, antiprotons (\bar{p} 's) and p 's are ideal [3] for understanding drift effects under the change in overall modulation level, because they are different only in charge sign.

In the last solar minimum period, the BESS experiment revealed that the cosmic-ray \bar{p} spectrum has a distinct peak around 2 GeV [6], which is a characteristic feature of secondary \bar{p} 's produced by cosmic-ray interactions with interstellar (IS) gas. It has become evident

that \bar{p} 's are predominantly secondary in origin, because several recent calculations of the secondary spectrum basically agree with observations in their absolute values and spectral shapes [3,4,7,8].

We report here new measurements of cosmic-ray \bar{p} and p fluxes and their ratios in the energy range from 0.18 to 4.2 GeV collected in two BESS balloon flights carried out in 1999 and 2000, when the solar activity was maximum. Based on the solar magnetic field data [9], the Sun's polarity reversed between these two flights [10]. With our full set of data [6,11–13], we discuss the temporal variation of the \bar{p} flux and \bar{p}/p ratio covering the solar minimum, the maximum, and the field reversal.

The BESS spectrometer was designed [14,15] and developed [16–19] as a high-resolution spectrometer. A uniform field of 1 Tesla is produced by a thin superconducting solenoid [20], and the field region is filled with tracking detectors. This geometry results in an acceptance of 0.3 m²sr. Tracking is performed by fitting up to 28 hit-points in drift chambers, resulting in a magnetic-rigidity ($R \equiv Pc/Ze$) resolution of 0.5% at 1 GV. The upper and lower scintillator-hodoscopes [19] provide time-of-flight and two dE/dx measurements. Time resolution of each counter is 55 ps, resulting in a $1/\beta$ resolution of 0.014, where β is defined as particle velocity normalized by the speed of light. The instrument also incorporates a threshold-type Cherenkov counter [18] with a silica-aerogel radiator ($n=1.02$) that can reject e^- and μ^- backgrounds by a factor of 4000 and identify \bar{p} 's from such backgrounds up to 4.2 GeV. In addition to biased trigger modes [13,17] selecting negatively-charged particles preferentially, one of every 60 (30) first-level triggered events were recorded to provide unbiased samples

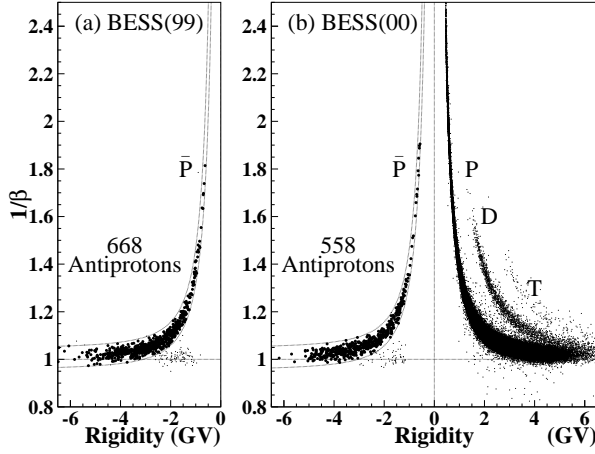


FIG. 1. The identification plots of \bar{p} events for (a) 1999 and (b) 2000 flights. The dotted curves define the \bar{p} mass bands.

in 1999 (2000). Note that the first-level trigger was provided by a coincidence between the top and bottom scintillators, with the threshold set at $1/3$ of the pulse height from minimum ionizing particles.

The experiments were carried out in northern Canada, Lynn Lake to Peace River, where the geomagnetic cutoff rigidity ranges from 0.3 to 0.5 GV. Data for flux measurements were taken for live-time periods of 100,471 and 90,765 sec at altitudes above 34 km (residual air of 4.3 and 5.0 g/cm^2 on average) in 1999 and 2000, respectively. Data during ascent were also collected at various altitudes, in order to estimate a background from atmospheric secondary p 's.

Analysis was performed in the same way as described in Ref. [13]. We applied the same selection criteria for \bar{p} 's and p 's because non-interacting \bar{p} 's behave like p 's except for deflection in the symmetrical configuration of BESS. Figure 1 shows β^{-1} versus R plots for surviving events (for 1999, only the negative rigidity side is shown). We see clean narrow bands of 668 and 558 \bar{p} candidates at the exact mirror position of the p 's for the 1999 and

2000 data, respectively. The \bar{p} bands are slightly contaminated by e^- and μ^- backgrounds due to inefficiency of the aerogel Cherenkov counter, while contamination on the p band was negligible. We estimated the fraction of e^- and μ^- backgrounds to be 0 % (0 %), 0.6 % (0.5 %), and 2.3 % (1.5 %), respectively, at 0.3, 2, and 4 GeV for 1999 (2000) data. Other backgrounds such as albedo, mis-measured positive-rigidity particles, and “re-entrant albedo” were found to be negligible.

The survival probabilities for \bar{p} 's and p 's to traverse residual air and the instrument without interactions and to pass through all the selection criteria described above were estimated by a Monte Carlo (MC) simulation. The MC code was tuned and verified by comparing the simulation with an accelerator beam test of the BESS detector [21]. The systematic uncertainty of the \bar{p} interaction losses were reduced to 5 %. Estimates of the background from atmospheric secondary \bar{p} 's were calculated [22–24] with the p and He fluxes measured by BESS as input. The subtraction amounts to 15 ± 5 % (17 ± 6 %), 23 ± 2 % (30 ± 2 %), and 26 ± 8 % (28 ± 9 %) for 0.3, 2, and 4 GeV in 1999 (2000), respectively, where the errors correspond to the maximum difference among the calculations. The background from atmospheric secondary p 's was estimated according to the calculation [25]. The parameters used in the calculation were tuned and verified [26] by comparing the calculated fluxes at various air depths with the atmospheric growth curve of p 's measured by BESS. The subtraction amounts to 27 ± 4 % (55 ± 8 %), 10 ± 2 % (22 ± 3 %), and 4 ± 1 % (8 ± 1 %) for 0.2, 0.5, and 1 GeV in 1999 (2000), respectively, where the errors correspond to the maximum difference between observed and calculated atmospheric growth curve of the p 's. Table I gives the resultant fluxes of \bar{p} 's and p 's and their flux ratios, \bar{p}/p , at the top of the atmosphere (TOA) with the statistical (first) and systematic (second) errors.

Figure 2 shows the \bar{p} and p fluxes in 1999 and 2000, together with the data [6] taken in 1997 at the solar minimum period. The error bars represent quadratic sums of

TABLE I. Antiproton fluxes (in $10^{-2} \text{ m}^{-2} \text{ s}^{-1} \text{ sr}^{-1} \text{ GeV}^{-1}$), proton fluxes (in $10^2 \text{ m}^{-2} \text{ s}^{-1} \text{ sr}^{-1} \text{ GeV}^{-1}$), and \bar{p}/p ratio (in unit of 10^{-5}) at TOA. T (in GeV) defines the kinetic energy bins. $N_{\bar{p}}$ is the number of observed antiprotons.

T (GeV)	BESS 1999				BESS 2000			
	$N_{\bar{p}}$	\bar{p} flux	p flux	\bar{p}/p ratio	$N_{\bar{p}}$	\bar{p} flux	p flux	\bar{p}/p ratio
0.18 - 0.28	2	$0.22^{+0.28+0.02}_{-0.15-0.02}$	$10.42^{+0.09+1.01}_{-0.09-1.01}$	$0.21^{+0.26+0.02}_{-0.14-0.02}$	7	$0.75^{+0.41+0.08}_{-0.34-0.08}$	$1.71^{+0.04+0.35}_{-0.04-0.35}$	$4.38^{+2.37+0.94}_{-1.97-0.94}$
0.28 - 0.40	9	$0.57^{+0.28+0.04}_{-0.20-0.04}$	$11.79^{+0.07+0.60}_{-0.07-0.60}$	$0.49^{+0.24+0.04}_{-0.17-0.04}$	6	$0.40^{+0.26+0.03}_{-0.18-0.03}$	$2.28^{+0.03+0.22}_{-0.03-0.22}$	$1.76^{+1.16+0.21}_{-0.77-0.21}$
0.40 - 0.56	28	$1.25^{+0.31+0.07}_{-0.27-0.07}$	$11.76^{+0.06+0.44}_{-0.06-0.44}$	$1.07^{+0.26+0.06}_{-0.23-0.06}$	8	$0.29^{+0.19+0.04}_{-0.16-0.04}$	$2.62^{+0.02+0.14}_{-0.02-0.14}$	$1.12^{+0.74+0.17}_{-0.60-0.17}$
0.56 - 0.78	27	$0.71^{+0.22+0.07}_{-0.20-0.07}$	$10.51^{+0.05+0.31}_{-0.05-0.31}$	$0.67^{+0.21+0.06}_{-0.19-0.06}$	36	$1.09^{+0.27+0.08}_{-0.23-0.08}$	$2.74^{+0.02+0.10}_{-0.02-0.10}$	$4.00^{+0.99+0.29}_{-0.83-0.29}$
0.78 - 1.10	63	$1.20^{+0.21+0.07}_{-0.20-0.07}$	$8.76^{+0.03+0.25}_{-0.03-0.25}$	$1.37^{+0.24+0.08}_{-0.22-0.08}$	67	$1.35^{+0.24+0.08}_{-0.22-0.08}$	$2.64^{+0.01+0.08}_{-0.01-0.08}$	$5.11^{+0.90+0.30}_{-0.84-0.30}$
1.10 - 1.53	112	$1.85^{+0.24+0.11}_{-0.23-0.11}$	$6.70^{+0.03+0.20}_{-0.03-0.20}$	$2.77^{+0.36+0.16}_{-0.34-0.16}$	77	$1.20^{+0.21+0.08}_{-0.19-0.08}$	$2.37^{+0.01+0.07}_{-0.01-0.07}$	$5.05^{+1.07+0.32}_{-0.82-0.32}$
1.53 - 2.15	138	$1.89^{+0.22+0.11}_{-0.21-0.11}$	$4.60^{+0.02+0.16}_{-0.02-0.16}$	$4.12^{+0.48+0.23}_{-0.46-0.23}$	102	$1.33^{+0.20+0.08}_{-0.19-0.08}$	$1.92^{+0.01+0.08}_{-0.01-0.08}$	$6.95^{+1.07+0.44}_{-1.00-0.44}$
2.15 - 3.00	162	$1.70^{+0.18+0.13}_{-0.17-0.13}$	$2.90^{+0.01+0.11}_{-0.01-0.11}$	$5.86^{+0.63+0.42}_{-0.60-0.42}$	131	$1.32^{+0.17+0.11}_{-0.16-0.11}$	$1.44^{+0.01+0.05}_{-0.01-0.05}$	$9.20^{+1.18+0.78}_{-1.12-0.78}$
3.00 - 4.20	127	$1.20^{+0.15+0.18}_{-0.14-0.18}$	$1.70^{+0.01+0.06}_{-0.01-0.06}$	$7.05^{+0.90+0.98}_{-0.85-0.98}$	124	$1.19^{+0.16+0.19}_{-0.15-0.19}$	$1.00^{+0.01+0.04}_{-0.01-0.04}$	$11.93^{+1.59+1.79}_{-1.50-1.79}$

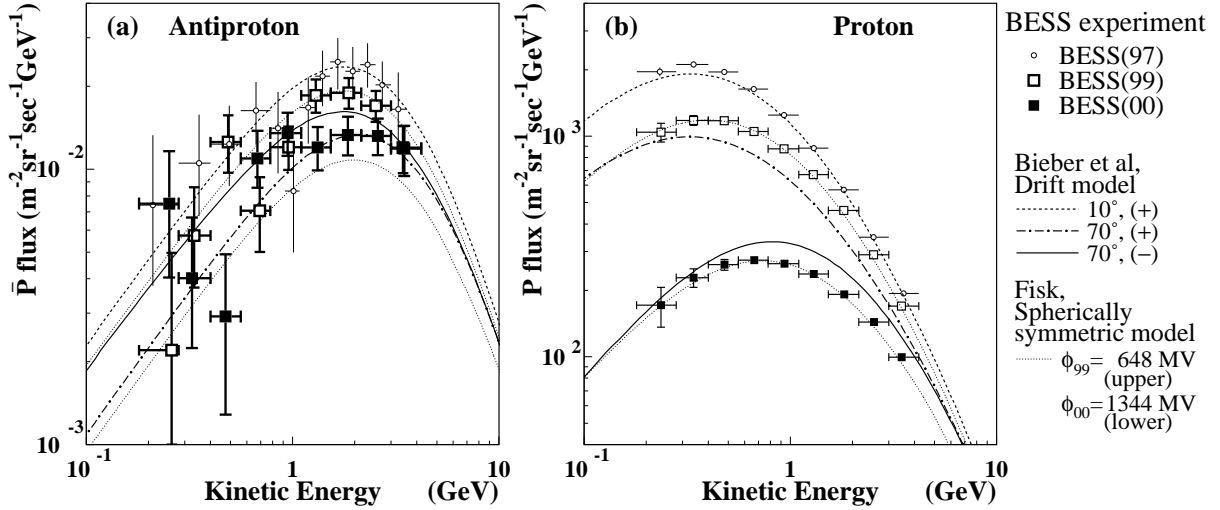


FIG. 2. The (a) \bar{p} and (b) p fluxes at TOA measured by BESS in 1999 and 2000 together with the previous data in 1997. The curves represent the calculations by the drift model [3] at a period of 10° (+), 70° (+), and 70° (-), which respectively represent solar minimum at positive phase (dashed line), solar maximum at positive phase (dash-dotted line), and solar maximum at negative phase (solid line). The dotted curves represent the calculations by the spherically symmetric model [27].

the statistical and systematic errors, as well as in the following figures. The dotted curves represent the modulated spectra according to the standard spherically symmetric approach [27], in which the modulation is characterized by a single parameter (ϕ) irrespective of the Sun's polarity. In each year, ϕ was determined to fit the p spectrum measured by BESS assuming the IS spectrum in Ref. [3]. The same ϕ was applied to modulate the \bar{p} flux. In both plots, dashed, dash-dotted, and solid curves represent modulated spectra according to a steady-state drift model [3] in which the modulation is characterized by a tilt angle (α) of the heliospheric current sheet and the Sun's magnetic polarity (denoted as $+/-$). Note that periods at 10° (+), 70° (+), and 70° (-) roughly correspond to the years of 1997, 1999, and 2000, respectively. However, it is shown in Fig. 2 that the actual level of overall modulation at the date of observation was lower (corresponding to a smaller value of α) in 1999 and higher (larger α) in 2000. Thus, the predicted effect of the drifts in Fig. 2(a) might be hidden under the change in overall modulation level. The drift model needs to be fine-tuned to reproduce the \bar{p} and p spectra. The retardation of the modulation effect due to the gradually expanding heliospheric current sheet [28] might also be concerned.

Figure 3 shows the \bar{p}/p ratios in 1999 and 2000 in which the above mentioned difficulty is partly canceled. In general, \bar{p} 's suffer less modulation than p 's because of their relatively hard IS spectrum. Thus, the spherically symmetric model predicts an increase in \bar{p}/p towards the solar maximum period [29], mainly due to a decrease of the p flux. The drift model predicts a much larger increase in \bar{p}/p reflecting the charge-sign dependence. It should be noted that a recent independent work [4] has shown qualitatively the same feature in \bar{p}/p while these two drift model calculations were different in IS spectra

and some modulation parameters. As shown in Fig. 3, the measured \bar{p}/p ratios are in better agreement with the drift model than the spherically symmetric model.

Combining all the previous BESS measurements since 1993 [6,11–13], annual variations of the \bar{p}/p ratios (relative to the ratio in IS) at energies of 0.2 – 0.4 GeV (closed square, denoted as 0.3 GeV), 0.8 – 1.3 GeV (open circle, 1.0 GeV), and 1.5 – 2.5 GeV (closed star, 1.9 GeV) are shown in Fig. 4(a). These data show no distinctive year-to-year variation before the solar field reversal indicated by the shaded area in Fig 4(a). The curves represent calculations of the \bar{p}/p time variation according to the drift model (dashed) and the spherically symmetric

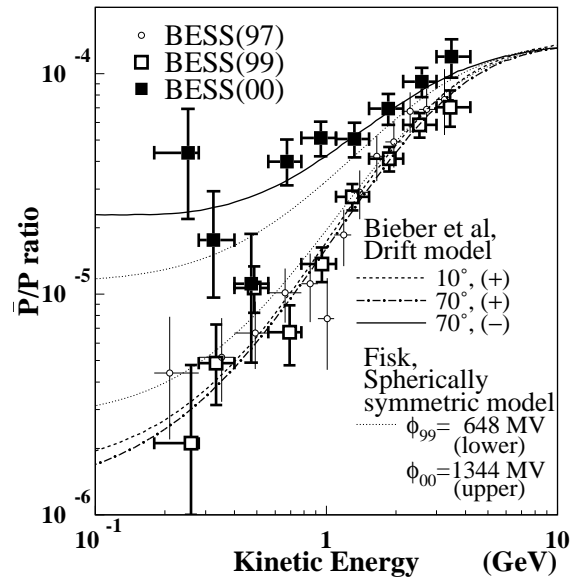


FIG. 3. The \bar{p}/p flux ratios measured by BESS in 1999 and 2000 with the previous data in 1997. The curves are calculations of the ratio at various solar activity [3,27].

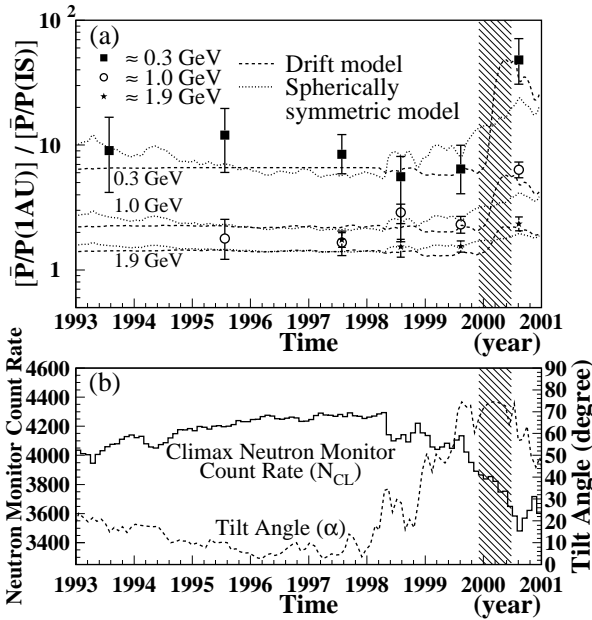


FIG. 4. (a) Temporal variation of the \bar{p}/p ratios (relative to the ratio in IS) at 0.3 (closed squares), 1.0 (open circles), and 1.9 GeV (closed stars) measured by BESS since 1993. Curves represent the calculated temporal variation of the ratios (see text). (b) Temporal variation of N_{CL} and α . In both plots, shaded area indicates the period of the solar field reversal.

model (dotted) for 0.3, 1.0, and 1.9 GeV from top to bottom. We obtained those ϕ 's at the dates of the BESS flights (ϕ_{BESS}) and then we evaluated ϕ 's at any moments using a linear relation between ϕ_{BESS} and N_{CL} , where N_{CL} is the monthly averaged count rates of the Climax Neutron Monitor [30]. The historical trend of N_{CL} is indicated by the solid histogram in Fig. 4(b). In Ref. [3], the \bar{p}/p ratios are given as a function of the tilt angle, α , rather than the actual time. In order to draw the dashed curve in Fig. 4(a), we take α as the mean position of the maximum latitudinal extent of the current sheet [31] taking no account of the retardation of the modulation effect. Note that α is allowed to reach 90° in the shaded area to avoid discontinuity in \bar{p}/p at the field reversal. The drift model predicts that the \bar{p}/p ratio is stable during the positive phase and shows a sudden increase after the positive-to-negative solar field reversal. Our measurements generally agree with the drift model.

As a conclusion, we have measured the temporal variation of the \bar{p} and p fluxes covering the solar minimum, the maximum, and the solar magnetic field reversal. We observed stable \bar{p}/p ratios in the positive polarity phase through 1999 and a sudden increase in 2000 following the solar field reversal. The continuous observation has enabled a crucial test of drift effects in the solar modulation including a solar maximum period. It will motivate further development of models with more realistic parameters [4] and time dependence [32]. Furthermore, detailed understanding of solar modulation is inevitably important for investigating the origin of \bar{p} 's [33], especially in

the very low energy region below 0.5 GeV, where slightly excessive \bar{p} fluxes relative to the theoretical calculations were observed during the solar minimum [6,12].

We thank NASA and NSBF for the balloon expedition, and KEK and ISAS for continuous support. This work was supported by Grant-in-Aid for Scientific Research, MEXT in Japan; and by NASA in the USA. Analysis was performed using the computing facilities at ICEPP, the University of Tokyo.

* deceased.

† Present address: University of Tsukuba, Japan.

‡ Present address: Tohoku University, Japan.

- [1] J.R. Jokipii *et al.*, *Astrophys. J.* **243**, 1115 (1981).
- [2] R. A. Burger *et al.*, *Astrophys. J.* **505**, 244 (1998).
- [3] J. W. Bieber *et al.*, *Phys. Rev. Lett.* **83**, 674 (1999); *Proc. 26th Int. Cosmic Ray Conf. (Utah)* **7**, 17 (1999).
- [4] I. V. Moskalenko *et al.*, astro-ph/0106567.
- [5] M. Garcia-Munoz *et al.*, *Proc. 22nd Int. Cosmic Ray Conf. (Dublin)* **3**, 497 (1991); A. Raviart *et al.*, *Proc. 25th Int. Cosmic Ray Conf. (Durban)* **2**, 37 (1997).
- [6] S. Orito *et al.*, *Phys. Rev. Lett.* **84**, 1078 (2000).
- [7] L. Bergström *et al.*, *Astrophys. J.* **526**, 215 (1999).
- [8] F. Donato *et al.*, astro-ph/0103150.
- [9] the Wilcox Observatory at Stanford, <http://quake.stanford.edu/~wso/Polar.ascii>.
- [10] J. Clem and Paul Evenson, *Proc. 27th Int. Cosmic Ray Conf. (Hamburg)* 3934 (2001).
- [11] K. Yoshimura *et al.*, *Phys. Rev. Lett.* **75**, 3792 (1995); A. Moiseev *et al.*, *Astrophys. J.* **474**, 479 (1997).
- [12] H. Matsunaga *et al.*, *Phys. Rev. Lett.* **81**, 4052 (1998).
- [13] T. Maeno *et al.*, *Astropart. Phys.* **16**, 121 (2001).
- [14] S. Orito, *Proc. of the ASTROMAG Workshop, KEK Report 87-19*, 111 (1987).
- [15] A. Yamamoto *et al.*, *IEEE Trans. Magn.* **24**, 1421 (1988).
- [16] A. Yamamoto *et al.*, *Adv. Space Res.* **14**(2), 75 (1994).
- [17] Y. Ajima *et al.*, *Nucl. Instr. Meth. A* **443**, 71 (2000).
- [18] Y. Asaoka *et al.*, *Nucl. Instr. Meth. A* **416**, 236 (1998).
- [19] Y. Shikaze *et al.*, *Nucl. Instr. Meth. A* **455**, 596 (2000).
- [20] Y. Makida *et al.*, *IEEE Trans. Applied Supercon.* **5**(2), 638 (1995).
- [21] Y. Asaoka *et al.*, *Proc. 27th Int. Cosmic Ray Conf. (Hamburg)* 2139 (2001).
- [22] T. Mitsui, Ph.D. thesis, University of Tokyo, 1996.
- [23] S. A. Stephens *et al.*, *Astropart. Phys.* **6**, 229 (1997).
- [24] Ch. Pfeifer *et al.*, *Phys. Rev. C* **54**, 882 (1996).
- [25] P. Papini *et al.*, *Nuovo Cimento* **19**, 367 (1996).
- [26] Y. Shikaze *et al.*, (in preparation): In the calculation code of atmospheric protons, the recoil production spectrum [25] was modified to reproduce the p flux during ascent.
- [27] L. A. Fisk, *J. Geophys. Res.* **76**, 221 (1971).
- [28] J.A. le Roux *et al.*, *Astrophys. J.* **361**, 275 (1990).
- [29] A.W. Labrador *et al.*, *Astrophys. J.* **480**, 371 (1997).
- [30] <http://odysseus.uchicago.edu/NeutronMonitor/>: University of Chicago, NSF Grant ATM-9613963.
- [31] Hoeksema, <http://quake.stanford.edu/~wso/Tilts.html>.
- [32] R.A. Burger *et al.*, *Proc. 27th Int. Cosmic Ray Conf. (Hamburg)*, 3835 (2001).
- [33] A. Yamamoto *et al.*, *Adv. Space Res.*, in press.